Applied Surface Science 292 (2014) 219–224

Contents lists available at ScienceDirect

Applied Surface Science

journal homepage: www.elsevier.com/locate/apsusc

Influence of oxygen pressure on the structural, electrical and optical properties of Nb-doped ZnO thin films prepared by pulsed laser deposition

Muying Wu [a,*], Shihui Yu [b], Lin He [a], Geng Zhang [a], Dongxiong Ling [a], Weifeng Zhang [c]

[a] School of Electronic Engineering, Dongguan University of Technology, Guangdong Dongguan 523808, China
[b] School of Electronic and Information Engineering, Tianjin University, Tianjin 300072, China
[c] Key Laboratory of Photovoltaic Materials of Henan Province and School of Physics and Electronics, Henan University, Kaifeng 475004, China

ARTICLE INFO

Article history:
Received 4 June 2013
Received in revised form 17 October 2013
Accepted 21 November 2013
Available online 1 December 2013

Keywords:
NZO
Pulsed laser deposition
Oxygen pressure
TCO

ABSTRACT

Nb-doped zinc oxide (NZO) transparent conductive thin films with highly (0 0 2)-preferred orientation were deposited on glass substrates by pulsed laser deposition method in oxygen ambience under different oxygen pressures. The as-deposited films were characterized by X-ray diffraction (XRD), Field emission-scanning electron microscopy (FE-SEM), electrical and optical characterization techniques. It was found that a desirable amount of oxygen can reduce the related defect scattering and enhance the carrier mobility. The resistivity and average optical transmittance of the NZO thin films are of 10^{-4} Ω cm and over 88%, respectively. The lowest electrical resistivity of the film is found to be about 4.37×10^{-4} Ω cm. In addition, the influence of oxygen pressure on optical properties in NZO thin films was systematically studied as well.

© 2013 Elsevier B.V. All rights reserved.

1. Introduction

Transparent conducting oxides (TCOs), owing to their high electrical conductivity and high optical transmittance in the visible, and high infrared reflectance [1–5], have been widely used as transparent electrodes in various fields such as solar cells, optoelectronic devices, flat panel displays, heat mirrors, and gas sensor. Compared with the more widely used indium tin oxide (ITO), ZnO thin films have lots of advantages, such as low cost, good thermal stability, and convenient fabrication, which show a big potential use for the various applications of solar cells[6], flat panel displays and so on.

Presently, many dopants, such as aluminium(Al) [2,3], gallium (Ga) [4], fluorine (F) [7], niobium (Nb) [8], manganese (Mn) [9], indium (In) [10], titanium (Ti) [11], zirconium (Zr) [12], tin (Sn) [13], boron (B) [5], bismuth (Bi) [14] and chlorine (Cl) [15], have been investigated to improve the electrical and optical properties of ZnO thin films. Among these, Nb doping in ZnO is quite attractive because there is a valence difference of 3 between Nb^{5+} and Zn^{2+}. Therefore, only a tiny amount of Nb doping can produce enough free carriers to reduce the ion scattering effect [16]. In addition, Nb doping also seems to be the most successful and promising due to its smaller ionic radius of 0.70 Å [17] (0.74 Å [18]), as compared with corresponding values of Zn given in parentheses. Furthermore, Nb has high thermal stability that is enhanced even further when doped into ZnO. As a result, ZnO-based TCO thin films have a great potential in numerous applications.

There are numerous deposition techniques used to grow ZnO thin films (either doped or undoped) including molecular beam epitaxy (MBE) [19], sol–gel processing [13], magnetron sputtering [3,5], metal–organic chemical vapor deposition (MOCVD) [15], thermal evaporation [20] and spray pyrolysis [10,12], and pulsed laser deposition (PLD) [2,4]. Among these fabrication methods, PLD provides several advantages for the growth of multi-component oxide thin films. The composition of films grown by PLD is quite close to that of the target, and it is true even for a multi-component target. Also, PLD films crystallize at relatively lower substrate temperatures compared to other physical vapor deposition (PVD) processes due to the high kinetic energies (>1 eV) of the ejected species in the laser produced plasma [21].

The low resistivity of ZnO thin films is due to defects of oxygen vacancies and zinc interstitials [22]. It is important to study the effect of oxygen pressure on its optoelectrical properties. Literature survey revealed that there was no report on effect of oxygen pressure on optoelectrical properties of Nb doped ZnO thin films by pulsed laser deposition technique. A key to achieve better electrical properties may lie in a good understanding of the role of oxygen in this material system. Therefore in this paper, we study the effects of oxygen pressure on structural, electrical and optical properties of Nb-doped ZnO thin films.

* Corresponding author. Tel.:+86 769 22861102.
E-mail addresses: wumy@dgut.edu.cn, wumy01@163.com (M. Wu).

0169-4332/$ – see front matter © 2013 Elsevier B.V. All rights reserved.
http://dx.doi.org/10.1016/j.apsusc.2013.11.119

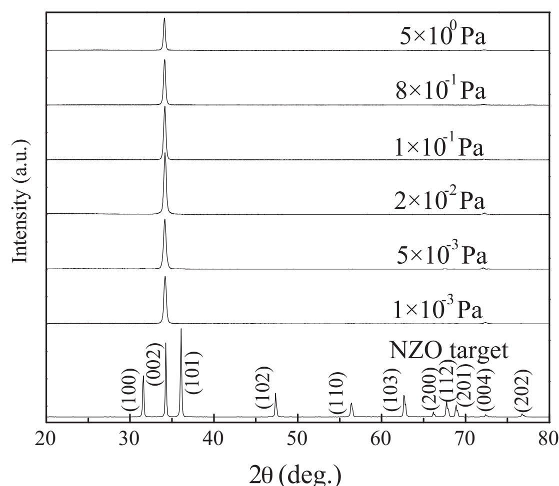

Fig. 1. X-ray diffraction patterns as a function of oxygen pressure for NZO thin films.

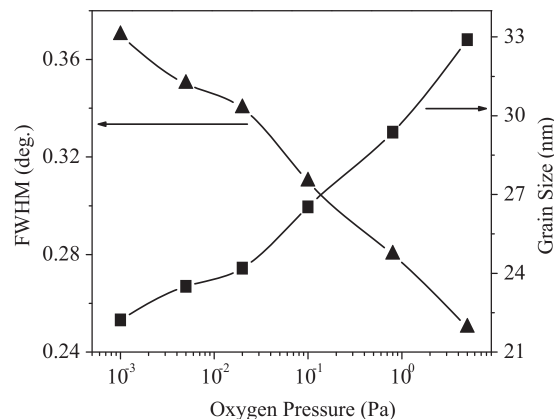

Fig. 2. Grain size and FWHM of (0 0 2) peak of NZO thin films prepared at various oxygen pressures.

2. Experimental

NZO thin films were deposited on glass substrates with PLD method. A KrF excimer laser (248 nm, 300 mJ, 5 Hz) was employed as the ablation source. The NZO targets were prepared from ZnO powder (purity 99.99%) and Nb_2O_5 powder (purity 99. 9%) in a mol proportion of 98:2. The materials are mixed in an agate mortar with fine grinding for 5 h, pressed into 50 mm diameter and 4 mm thickness pellet at a pressure of 20 tone and then sintered in an alumina crucible at 1150 °C for 8 h in air. The substrates were first cleaned with alcohol for 30 min, rinsed in de-ionized water and subsequently dried in a flowing nitrogen gas before being loaded into the chamber. Prior to irradiations, the deposition chamber is evacuated down to a base pressure of 2×10^{-4} Pa and then oxygen (99.99%) was used as the ambient gas. The NZO films were deposited onto the substrate at a temperature of 350 °C and under various oxygen pressures (10^{-3} to 5 Pa). The target–substrate distance was kept at 5 cm. The deposition time of 60 min was maintained. The laser repetition rate was 5 Hz and the energy per pulse was 500 mJ. Before deposition, the target was pretreated in O_2 atmosphere for 15 min to remove any impurity on the surface of the target. After deposition, the films deposited at higher temperature are cooled to room temperature at the same oxygen pressure. All of the films with a typical thickness of about 300 nm obtained from the step height measurement instrument.

To confirm the properties of the films, the XRD patterns were collected on a DX–2700 diffractometer with Cu $K\alpha$ radiation (λ = 1.5418 Å), the room temperature Hall effect measurements were carried out using a Hall Effect measurement system (Ecopia HMS-3000), the surface morphologies were investigated by scanning electron microscopy (JEOL JSM-7600F, Akishima, Tokyo, Japan) and the transmittance of the films in the wavelength range 300–800 nm was measured using an ultraviolet–visible–near infrared (UV–Vis–NIR) spectrophotometer (Varian Cary 5000).

3. Results and discussions

Fig. 1 shows the XRD patterns of Nb: ZnO (NZO) thin films deposited under various oxygen pressures. All the samples exhibit (0 0 2) preferred orientation due to a self-texturing mechanism as discussed by Jiang et al. [23], which indicates that all the films are highly c-axis oriented. The texture coefficients of oxygen pressures of 10^{-3}, 5×10^{-3}, 2×10^{-2}, 1×10^{-1}, 8×10^{-1} and 5 Pa are 57.3%, 58.1%, 62.3%, 71.6%, 68.3% and 66.1%, respectively. With the increment of the oxygen pressure, the (0 0 2) peak intensity initially increases, to a maximum at 2×10^{-2} Pa, and then decreases gradually. No extra peaks due to the addition of niobium in zinc oxide films were observed, indicating the absence of an impurity phase in the films. That is, the diffractograms provide evidence of single phase crystalline zinc oxide (wurtzite structure).

These phenomenons can be explained as follows. For NZO thin films deposited at low oxygen pressure, there exist lots of oxygen vacancies, thus resulting in the fact that the chemical composition of them is non-stoichiometric and then they have worse crystalline. The excess of oxygen might induce defects in the NZO thin films, which interfere with the nucleation and growth of the films, thus lead to the degradation of the crystalline quality. In addition, the adatoms, with a smaller diffusion path length at higher oxygen pressure, will have less time to adopt a preferred in-plane orientation. Understandably, this reduction in surface adatom mobility can also lead to poor crystallinity. In our experiment, the condition of oxygen pressure at 2×10^{-2} Pa has produced the most highly oriented NZO films, being the critical oxygen partial pressure.

Fig. 2 displays FWHM (Full Width at Half Maximum) of NZO thin films grown at various oxygen pressures. The value of FWHM for the films decreases significantly with the increase of the oxygen pressure. The decrease of the FWHM indicates the increase of grain size of the NZO films. In order to attain the detailed structure information, we calculated the grain size along the c-axis according to the Scherrer's formula [24,25]

$$D = \frac{0.9\lambda}{\beta \cos\theta} \quad (1)$$

where D is the mean grain size, λ is the wave length of Cu $K\alpha$ radiation (1.5418 Å), β is the (0 0 2) peak width and θ is the Bragg diffraction angle. We have corrected β by considering the effect of instrumental broadening. The grain sizes of the thin films deposited at various oxygen pressures are plotted in Fig. 2. The D values increase from 22 to 33 nm with the increase of oxygen pressure, due to the interaction and agglomeration with each other at high oxygen pressure.

Surface morphology of the NZO thin films prepared at different oxygen pressures are studied by SEM. The SEM images in Fig. 3 indicate that the surface morphology is strongly dependent on the oxygen pressure. The average particle size of the NZO film is relatively small when prepared at a low oxygen pressure. With the increasing of oxygen pressure, the average particle size of the NZO film increased. This consists well with the above XRD analysis results. Fig. 3(g) shows the cross-sectional SEM micrograph of the NZO thin film deposited at oxygen pressure of 2×10^{-2} Pa. According to the cross-section images, the film exhibits a columnar crystal

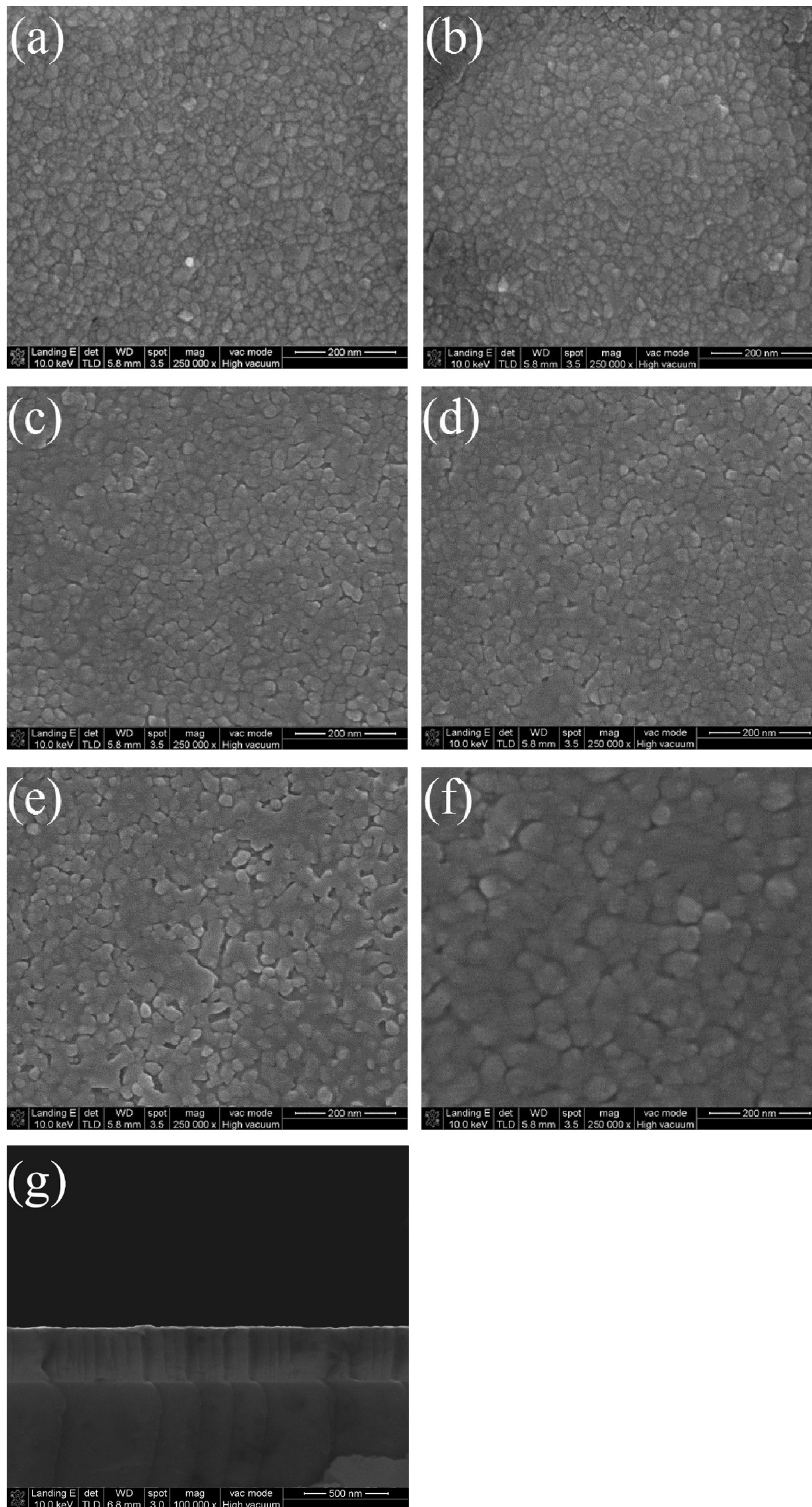

Fig. 3. SEM image of NZO thin films as a function of oxygen pressure for NZO thin films.

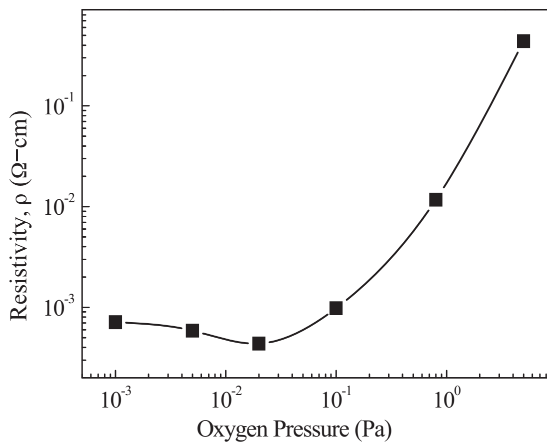

Fig. 4. Resistivity of NZO thin films as a function of oxygen pressure.

structure, with a thickness of about 300 nm, being consistent with the XRD measurement result.

In order to understand the relationship between oxygen pressure and electrical property of the film, the resistivity, carrier concentration and carrier mobility were measured by Hall measurement with the Van der Pauw method.

The variation of electrical resistivity as a function of oxygen pressure is shown in Fig. 4. The resistivity of the NZO films decreases when the oxygen pressure changes from 10^{-3} to 2×10^{-2} Pa. However, the resistivity rises gradually with the further increase in the oxygen pressure to 5 Pa. The change in resistivity of the NZO films with increasing oxygen pressures can be explained using the following basic relation [26]:

$$\rho = \frac{1}{ne\mu} \tag{2}$$

where ρ represents the resistivity, n represents the carrier concentration, e represents the charge of the carrier, and μ represents the mobility. From this equation, we see that changes in mobility and carrier concentration, both can affect the resistivity.

The corresponding carrier concentration and mobility of the NZO films are shown in Fig. 5. It is found that the carrier concentration increases first and then decreases as the oxygen pressure increased. In the low oxygen pressure regime (10^{-3} to 10^{-2} Pa), with the increase of the oxygen pressure, the carrier concentration increases from 6.06×10^{20} to 6.22×10^{20} cm^{-3}. In this oxygen deficient environment, although Zn antisites or Zn interstitials can be present as donor type defects [27], their formation energies are higher than those of oxygen vacancies [28], and so, oxygen

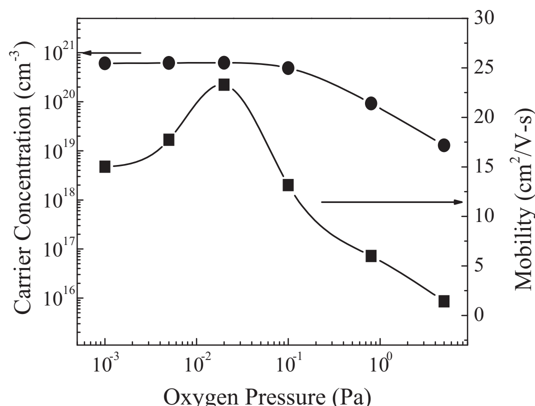

Fig. 5. Carrier concentration and Hall mobility of NZO thin films as a function of oxygen pressure.

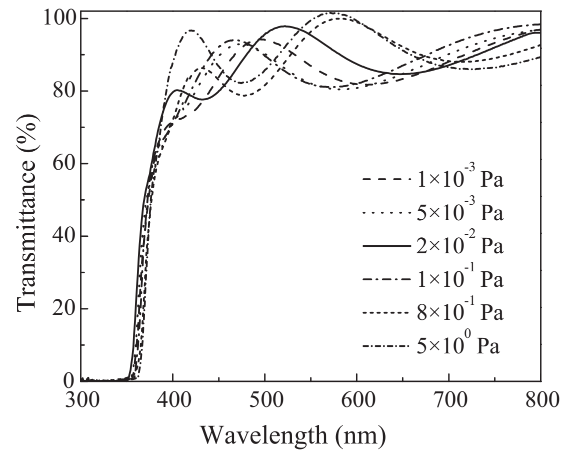

Fig. 6. Optical transmittance spectra of NZO thin films as a function of oxygen pressure.

vacancies represent the most stable defect formation [29]. This means that their absence or presence should not play a significant role in influencing the carrier concentration. This reason explains no significant change in our observation in the carrier concentrations. However, in the high oxygen pressure regime (10^{-2} to 5 Pa), with a further increase of the oxygen pressure to 5 Pa, it revealed that decreases in the carrier concentration. In this regime, oxygen interstitials have low formation energies especially in a higher oxidizing ambient [30]. Typically, oxygen interstitials can occupy the octahedral, tetrahedral, or the split interstitial sites [30]. When the octahedral sites are occupied, they tend to introduce states in the lower part of the band gap and these states can accept two electrons, therefore acting as compensation centers [30]. This can explain the decrease in the carrier concentration and the decreasing trend with increasing oxygen pressure.

The Hall mobility is expressed as [31]

$$\frac{1}{\mu} = \frac{1}{\mu_{GB}} + \frac{1}{\mu_{IS}} \tag{3}$$

where μ_{GB} is mobility of grain boundary scattering, μ_{IS} is mobility of ionized impurity scattering. It can be seen that in the low oxygen pressure regime, the mobility of the NZO films increases with the oxygen pressure. At a low oxygen pressure, the mobility of the films is limited, mainly due to the scattering from the grain boundaries and ionized defect scattering centers. There are more grain boundaries and ionized defect scattering centers due to small grain and poor crystallinity at a low oxygen pressure. With an increase in the oxygen pressure from 10^{-3} to 2×10^{-2} Pa, the mobility increases, reaches a maximum value (23.29 cm^2 V^{-1} s^{-1}) at 2×10^{-2} Pa, which can be attributed to reduced ionized defect scattering centers in the bulk film although grain boundaries passivation by oxygen can be a possible reason. With a further increase of the oxygen pressure to 5 Pa, the mobility drastically decreases to 1.42 cm^2 V^{-1} s^{-1}. In this process, the presence of highly disordered rotation of the crystal grains of the NZO forms added grain boundaries with poorer passivation and interfaces [30]. These are sources for significant grain boundary scatterings that can explain the drastic decrease in the mobility. In addition, as for oxygen interstitial occupying split sites (the tetrahedral site is unstable), the sharing of the lattice site with one of the nearest neighbors can produce a charge state of 1^+ [29]. The increase in ionized scattering through these defect centers then lowers the mobility of the conduction electrons.

Fig. 6 shows the dependence of the optical transmission of the NZO thin films in the wavelength region 300–800 nm as a function

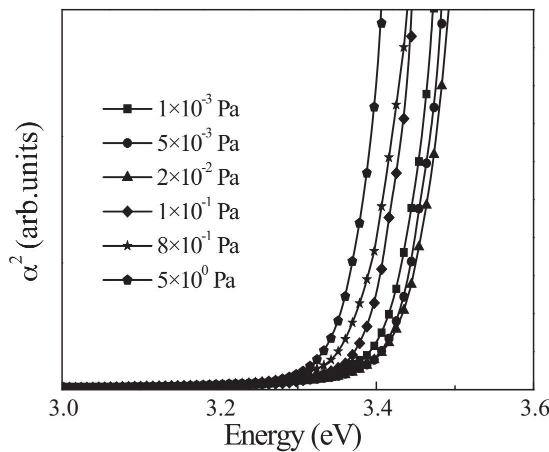

Fig. 7. Plots of $(\alpha)^2$ vs. $h\nu$ for the NZO thin films as a function of oxygen pressure.

of oxygen pressure. To determine the average transmittance T_{av}, the following relationship is used: [32]

$$Tav = \frac{\int V(\lambda)T(\lambda)d\lambda}{\int V(\lambda)d\lambda} \quad (4)$$

where $T(\lambda)$ represents the transmittance and $V(\lambda)$ represents the photopic luminous efficiency function defining the standard observer for photometry [33]. It is observed that all the NZO thin films exhibit a high transmittance in the visible region, regardless of the different oxygen pressure. The interference phenomenon, observed in every spectrum, indicates a smooth and homogeneous surface of the film. The average optical transmittance values of oxygen pressures of 10^{-3}, 5×10^{-3}, 2×10^{-2}, 1×10^{-1}, 8×10^{-1} and 5 Pa are 86.9%, 87.1%, 88.7%, 88.8%, 89.4% and 91.0%, respectively. It is observed that the average optical transmittance increases with the increase in the oxygen pressure. Due to the optical transmission of a film is strongly depending on its structure, surface morphology and density, the increase of the optical transmittance of NZO film with the increase of oxygen pressure can be attributed to a weakening of the scattering and the absorption of light with the increase of the grain size. In addition, since surface state is related to deep level defects, which are most probably due to oxygen vacancies or zinc interstitials, the surface state level will absorb visible photons [34]. But the surface state density of the NZO film greatly decreases with increasing oxygen pressure (as shown in Fig. 3), so the optical transmittance increases. Thus it can be seen that decrease of surface state density can further increase the optical transmittance.

The optical band gap of the films is calculated from the transmittance spectra. The absorption coefficient α is calculated using the following equation [35]

$$\alpha = \frac{\ln(1/T)}{d} \quad (5)$$

where d is the film thickness, α is the absorption coefficient and T is the transmittance of the film. The fundamental absorption, which corresponds to the electron excitation from valance band to conduction band, is usually used to determine the value of optical band gap Eg using the Tauc relationship [36],

$$a h\nu = C(h\nu - Eg)^n \quad (6)$$

where C is a constant, ν is the photon's frequency and the exponent n characterizes the nature of band transition. In this work, the value of n is 0.5 because the NZO film is a direct transition material. The curves of α^2 versus photon energy are plotted in Fig. 7. The optical band-gap was determined by extrapolating the straight regions of the plots of α^2 vs. $h\nu$ to $\alpha^2 = 0$ (i.e., $\alpha h\nu = 0$). As the oxygen pressure raises from 10^{-3} to 2×10^{-2} Pa, the optical band gap shifts to a short wavelength i.e. a high energy (blue shift), which is generally attributed to the Burstein–Moss shift [12,14,21,24]. The Fermi energy penetrates into the conduction band of the degenerate semiconductor, due to an increase in the carrier concentration, which leads to the energy band widening. With a further increase of the oxygen pressure to 5 Pa, the optical band-gap decreases. The decrease of carrier concentration, lead to the optical gap shortening because of the Burstein–Moss effect. Also another effect, the band gap renormalization due to many body effects may lead to a narrowing of the energy gap, which is needed to be taken into account. This band gap narrowing is competitive with the Burstein–Moss effects [37]. Two competing effects have made the complicated variation of the optical gap of AZO films.

4. Conclusions

Transparent conducting NZO films have been deposited by PLD on glass substrates. The structural, electrical and optical properties of NZO films were investigated under various oxygen pressures. The films are polycrystalline and have preferred orientation along [0 0 2] direction. The effects of oxygen pressure on the film properties were studied. The lowest resistivity of 4.37×10^{-4} Ω cm could be obtained at the oxygen pressure of 2×10^{-2} Pa. The average optical transmittance of the films is over 88%. Also the role of oxygen pressure on the electrical properties of NZO films was discussed. In addition, the influence of oxygen pressure on optical properties in NZO thin films was systematically studied. It was confirmed that pulsed laser deposited n-type transparent NZO can be applied to electrode as a potential good challenger to ITO films.

Acknowledgements

This project is supported by the Science and Technological Program for Dongguan's Higher Education, Science and Research, and Health Care Institutions (Grant no. 2011108102025) and the Major National Development Project of Scientific Instrument and Equipment, China (Grant no. 2012YQ1400511).

References

[1] T. Minami, Semicond. Sci. Technol. 20 (4) (2005) S35.
[2] C.A. Tseng, J.C. Lin, Y.F. Chang, S.D. Chyou, K.C. Peng, Appl. Surf. Sci. 258 (2012) 5996.
[3] P. Gondoni, M. Ghidelli, F. Di Fonzo, V. Russo, P. Bruno, J. Martí-Rujas, C.E. Bottani, A. Li Bassi, C.S. Casari, Thin Solid Films 520 (2012) 4707.
[4] V. Bhosle, A. Tiwari, J. Narayan, J. Appl. Phys. 100 (3) (2006) 033713.
[5] Q. Huang, Y. Wang, S. Wang, D. Zhang, Y. Zhao, X. Zhang, Thin Solid Films 520 (2012) 5960.
[6] Z. Zang, A. Nakamura, J. Temmyo, Opt. Express 21 (9) (2013) 11448–11456.
[7] X. Noirfalise, T. Godfroid, G. Guisbiers, R. Snyders, Acta Mater. 59 (2011) 7521.
[8] J.M. Lin, Y.Z. Zhang, Z.Z. Ye, Appl. Surf. Sci. 255 (2009) 6460.
[9] H. Zhang, R. Liu, H. Liu, C. Lei, D. Feng, C. Yuan, Mater. Lett. 64 (2010) 605.
[10] B.C. Jiao, X.D. Zhang, C.C. Wei, J. Sun, Q. Huang, Y. Zhao, Thin Solid Films 520 (2011) 1323.
[11] C.S. Wu, B.T. Lin, R.Y. Yang, Appl. Surf. Sci. 258 (2012) 9891.
[12] V. Gokulakrishnana, S. Parthibanb, K. Jeganathanc, K. Ramamurthia, Appl. Surf. Sci. 257 (2011) 9068.
[13] K.C. Yung, H. Liem, H.S. Choy, J. Phys. D: Appl. Phys. 42 (2009) 185002.
[14] F. Chouikh, Y. Beggah, M.S. Aida, J. Mater. Sci.—Mater. El. 22 (2011) 499.
[15] E. Chikoidze, M. Nolan, M. Modreanu, V. Sallet, P. Galtier, Thin Solid Films 516 (2008) 8146.
[16] H.K. Kim, S.H. Huh, J.W. Park, J.W. Jeong, G.H. Lee, Chem. Phys. Lett. 354 (2002) 165.
[17] Y.P. Yadava, M.M. de Lima, J.S. Oliveira, R.A. Sanguinetti Ferreira, Mater. Sci. Appl. 3 (2012) 408.
[18] R.D. Shannon, Acta Crystallogr. Section A 32 (5) (1976) 751–767.
[19] Z. Yang, D.C. Look, J.L. Liu, Appl. Phys. Lett. 94 (2009) 072101.
[20] R. Yousefi, M.R. Muhamad, A.K. Zak, Curr. Appl Phys. 11 (2011) 767.
[21] H. Kim, R.C.Y. Auyeung, A. Piqué, Thin Solid Films 516 (2008) 5052.
[22] B. Bayraktaroglu, K. Leedy, R. Bedford, Appl. Phys. Lett. 93 (2008) 022104.
[23] X. Jiang, C.L. Jia, B. Szyszka, Appl. Phys. Lett. 80 (2002) 3090.
[24] V. Khranovskyy, U. Grossner, O. Nilsen, V. Lazorenko, G.V. Lashkarev, B.G. Svensson, R. Yakimova, Thin Solid Films 515 (2006) 472.

[25] T. Ghosh, S. Bandopadhyay, K.K. Roy, A.K. Maiti, K. Goswami, Cryst. Res. Technol. 44 (2009) 879.
[26] A. Dhar, T.L. Alford, J. Appl. Phys. 112 (2012) 103113.
[27] F. Oba, A. Togo, I. Tanaka, Phys. Rev. B: Condens. Matter 77 (2008) 245202.
[28] A. Janotti, C.G. Van de Walle, Appl. Phys. Lett. 87 (2005) 122102.
[29] A. Janotti, C.G. Van de Walle, J. Cryst. Growth 287 (58) (2006).
[30] L.M. Wong, S.Y. Chiam, J.Q. Huang, S.J. Wang, J.S. Pan, W.K. Chim, Appl. Phys. Lett. 98 (2011) 022106.
[31] S.S. Lin, J.L. Huang, D.F. Lii, Mater. Chem. Phys. 90 (2005) 22.
[32] K. Sivaramakrishnan, T.L. Alford, Appl. Phys. Lett. 94 (2009) 052104.
[33] W.G. Driscoll, W. Vaughan, Handbook of Optics, McGraw-Hill, USA, 1978.
[34] W. Yang, Z. Wu, Z. Liu, A. Pang, Y.L. Tu, Z.C. Feng, Thin Solid Films 519 (2010) 31.
[35] D. Beena, K.J. Lethy, R. Vinodkumar, V.P. Mahadevan Pillai, V. Ganesan, D.M. Phase, S.K. Sudheer, Appl. Surf. Sci. 255 (2009) 8334.
[36] A. Ables, Optical Properties of Solids, North Holland, Amsterdam, 1992.
[37] J.G. Lu, S. Fujita, T. Kawaharamura, H. Nishinaka, Y. Kamada, T. Ohshima, Z.Z. Ye, Y.J. Zeng, Y.Z. Zhang, L.P. Zhu, H.P. He, B.H. Zhao, J. Appl. Phys. 101 (2007) 083705.